Eur. Phys. J A 447–453 (1998)

THE EUROPEAN PHYSICAL JOURNAL A


# Low–energy photodisintegration of $^9$Be and $\alpha + \alpha + n \leftrightarrow ^9$ Be $+\gamma$ reactions at astrophysical conditions

V.D. Efros[1], H. Oberhummer[2], A. Pushkin[3], I.J. Thompson[4]

[1] Russian Research Centre "Kurchatov Institute", Kurchatov Square 1, 123182 Moscow, Russia
[2] Institut für Kernphysik, Wiedner Hauptstrasse 8–10, TU Wien, A–1040, Vienna, Austria
[3] Department of Mathematical Physics, Lund Institute of Technology, P.O. Box, 118 S–221 00 Lund, Sweden
[4] Department of Physics, University of Surrey, Guildford GU2 5XH, United Kingdom

Received: 19 January 1998
Communicated by B. Povh

**Abstract.** A semi–microscopic model for the low–energy photodisintegration of the $^9$Be nucleus is constructed, and the experimental data are analyzed with its help. The older radioactive isotope data are supported by this analysis. The theoretical photodisintegration cross section is derived. The astrophysical rates for the reaction $\alpha + \alpha + n \rightarrow ^9$Be$+\gamma$ and the reverse photodisintegration of $^9$Be are calculated. The new reaction rate for $\alpha + \alpha + n \rightarrow ^9$Be$+\gamma$ is compared with previous estimations.

**PACS.** 25.20.Dc Photon absorption and scattering – 25.40.Lw Radioactive capture – 97.10.Cv Stellar structure, interiors, evolution, nucleosynthesis, ages – 21.60.Gx Cluster models – 21.45.+v Few-body systems

## I Introdution

Recently fully microscopic calculations of nuclei with $A \leq 9$ have become feasible [1,2]. The $^9$Be nucleus is such a system of special interest, as it allows tests of theories of interaction of composite particles [2]. The properties of low–energy continuum of $^9$Be are of particular importance in this connection. However, the corresponding experimental data on the low–energy photodisintegration of $^9$Be are not in mutual agreement (see Fig. 1). In the present work we develop a semi–microscopic model to describe the process, and we analyze the experimental data with its help. The model accounts simultaneously for both resonant and non–resonant contributions to the cross section. An estimation of the reliability of various data is obtained and a theoretical photodisintegration cross section is derived.

We also calculate the reaction rates of the reaction $^9$Be$+\gamma \rightarrow \alpha + \alpha + n$ and the reverse reaction for astrophysical conditions. These reaction rates are of relevance in the high–entropy bubble in type II supernovae, an astrophysical site that has been suggested for the r–process [3,4]. The baryonic matter in this bubble is dominated in the beginning by $\alpha$–particles, neutrons, and protons. The abundance distribution shifts then to higher masses through the recombination of the free $\alpha$–particles, neutrons, and protons. This generates the so–called $\alpha$–process leading to the formation of massive isotopes ($A \approx 100$). The reaction path in the $\alpha$–process is mainly determined by requirements of nuclear statistical equilibrium and depends also on the reaction rates of the various recombination paths bridging the mass 5 and 8 gaps. It has been shown that there are three principal reaction paths from

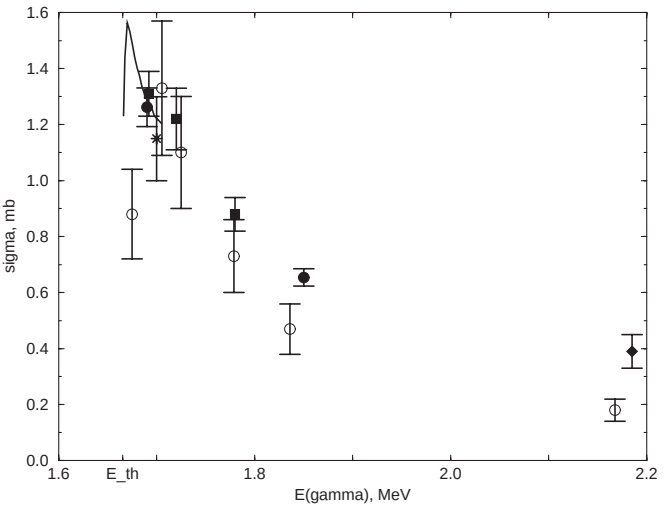


**Fig. 1.** Experimental data on the low–energy cross section for photodisintegration of $^9$Be. Bremsstrahlung data: Reference [12] (*solid curve* representing the fit of the authors to their data), [11] (*star* representing the maximum of the spectrum; the rest of the spectrum is not shown). Radioactive isotope data: Reference [13] (*full circles*), [14] (*full squares*), [15] (*full diamond*), [16] (*open circles*)

$^4$He to $^{12}$C:
(i) $^4$He($2\alpha$,$\gamma$)$^{12}$C
(ii) $^4$He($\alpha$n,$\gamma$)$^9$Be($\alpha$,n)$^{12}$C
(iii) $^4$He(2n,$\gamma$)$^6$He($\alpha$,n)$^9$Be($\alpha$,n)$^{12}$C.

It was shown in [4–6] that the triple–alpha process (i) can be neglected compared to the reaction sequence (ii) via $^9$Be under r–process conditions in the $\alpha$–process. Also the reaction path (iii) via $^6$He can be neglected for this scenario [6,7]. This is true even if the reaction rate of $^4$He(2n,$\gamma$)$^6$He is strongly enhanced [8], because then $^6$He is also destroyed very effectively through photodissociation. Therefore, for the $\alpha$– and r–process the reaction $^4$He($\alpha$n,$\gamma$)$^9$Be plays a key role in bridging the unstable mass gaps at $A = 5$ and $A = 8$.

The reaction rates of $^4$He($\alpha$ n,$\gamma$)$^9$Be and the reverse photodisintegration of $^9$Be were estimated in [9] from the experimental photodisintegration cross section. However, [9] did not include information on which experimental data their estimate was based. In view of the astrophysical relevance of these reactions we recalculate in the present work the rates of the first step of the reaction (ii) above.

The same problem is also addressed in [6]. These authors obtain the resonant contribution to the $^9$Be$(\gamma, n)^8$Be cross section from the Breit–Wigner formula for the first excited state of $^9$Be with the parameters taken from [10].[1] In order to calculate the non–resonant contribution they introduce a single–particle potential with the depth chosen to reproduce the ground state, calculate both ground– and final–state continuum wave functions in this potential, and multiply the cross section obtained by the shell–model spectroscopic factor. They then add this cross section constructively or destructively to the resonant cross section to establish possible upper and lower bounds for the reaction rates. This procedure has certain shortcomings: a resonant contribution to the cross section should not emerge as an addition to the dynamic model used, since a correct quantum mechanical model should necessarily contain such a contribution itself, along with the non–resonant contribution and an interference term. Besides, the potential wells used for the ground state and continuum state should in fact be different: an additional spin–orbit potential, for example, should be present in the ground p–state as compared to the continuum s–state.

In our model we use a three-body specification of the $^9$Be bound state, and a semimicroscopic continuum wave function which describes the essential scattering degrees of freedom at low relative energies. In Sect. 2 this model is formulated. In Sect. 3 the results for the $^9$Be$(\gamma, n)$ cross section are given. In Sect. 4 the astrophysical rates for $\alpha+\alpha+n \rightarrow ^9$Be$+\gamma$ and the reverse reaction are calculated.

[1] We note that the $\Gamma$ and $E_0$ parameters of the resonance used in [6] seem to be incorrect. The resonant properties of the $1/2^+$ state of $^9$Be will be considered in our future work.

## II The model

The relevant experimental data on the low–energy $^9$Be$(\gamma, n)$ cross section are presented in Fig. 1. The available data are those in [11,12] obtained with bremsstrahlung photons and those in [13–16] obtained from $\gamma$–radiation from radioactive isotopes. The peak at very low energy exhibited by the data of [12] is not confirmed by other groups, and may arise from discrepancies caused by neutron energy loss in the targets [17]. The radioactive isotope techniques normally provide more reliable results due to the absence of difficulties with the energy resolution. However, the cross section can be determined only for a few discrete photon energies with this method. This drawback will be cured below by the use of an appropriate theoretical model. Our strategy will be thus to analyze the radioactive isotope data. We shall consider the range of energies up to 0.5 MeV above threshold.

We need to obtain the ground state and continuum wave functions (WF) and calculate the transition matrix element. We start with the three–body $\alpha + \alpha + n$ representation of the $^9$Be system. Within this representation the WF in the c.m. system is the $\alpha\alpha n$ relative motion function times the intrinsic WFs of the two $\alpha$–particles. Since a predominant contribution to the transition matrix element comes from distances large compared to the size of the $\alpha$–particle additional antisymmetrization may be disregarded.[2] The intrinsic $\alpha$ particle WFs then will drop out from the calculation. In the following we shall refer to the three–particle relative motion function as to the WF of the system.

Let us denote $\boldsymbol{\rho}$ and $\mathbf{r}$ the distance between the $\alpha$ particles and that from their center of mass to the neutron, respectively. The ground state is $J^\pi = 3/2^-$, and its WF is of the form

$$\Psi_{\rm gs} = \sum_{l_1 l_2 L} \phi_{l_1 l_2 L}(\rho, r)[[Y_{l_1}(\hat{\rho})Y_{l_2}(\hat{r})]_L \chi_{1/2}]_J. \qquad (1)$$

Here $\chi$ is the neutron spin function, and the brackets $[\ldots]$ stand for angular momentum coupling. Because of the Pauli principle and parity requirements $l_1$ is even, and $l_2$ is odd. The WF in (1) was obtained from the three–body Schrödinger equation with $\alpha\alpha$ and $\alpha n$ potentials reproducing the observed two–body phase shifts. These potentials, along with some details of the calculation, are listed in the appendix. Practically an exact solution to the $\alpha+\alpha+n$ bound state problem is obtained, but one cannot get the experimental binding energy with these "bare" interparticle interactions. A possible reason is that the two $\alpha$–particles may distort each other in the $\alpha+\alpha+n$ bound state compared to the pure $n\alpha$ case. This may lead to a change in the $n\alpha$ interaction. To obtain a reasonable ground state WF the strength of the attractive central component of the $n\alpha$ potential is reduced by 8% in our calculation. This leads to values of 1.50 MeV and 2.48 fm for the binding energy and charge radius of $^9$Be, suffi-

[2] For example, the minor role of the antisymmetrization is seen from the calculations of the $\alpha + n + p$ system [18]

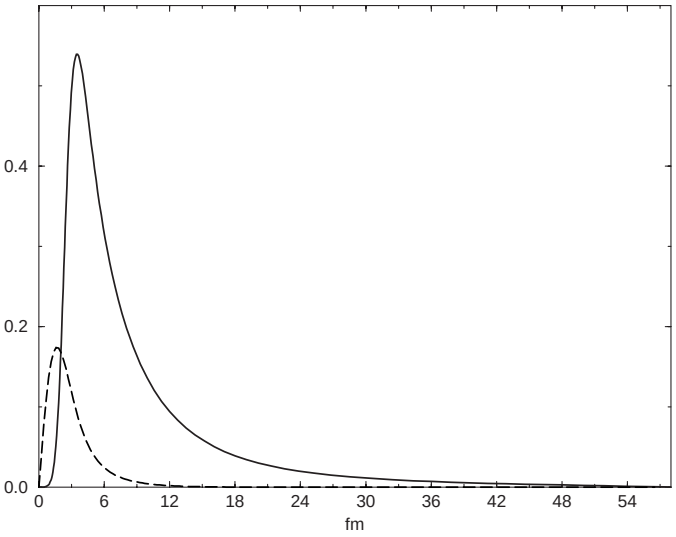


**Fig. 2.** The wave function of the $^8$Be resonance (*solid curve*) and the "effective" n–$^8$Be relative motion wave function in $^9$Be (*dashed curve*). The former wave function is constructed as the $s$–wave continuum solution in the $\alpha\alpha$ potential (see appendix) at the energy of 0.09518 MeV, the peak of the resonance in this potential

ciently close to the experimental values of 1.5736 MeV and $(2.51 \pm 0.01)$ fm.

Coming to the continuum wave function, we note first that the $^8$Be resonance produced in the reaction may be safely treated as a stable particle for the purposes of our calculation. This is because its width of 7 keV is extremely narrow on a nuclear scale. The $\alpha\alpha$ continuum wave function, taken at the resonance energy and normalized to unity in the interior region, decreases practically to zero in the Coulomb barrier region as shown in Fig. 2 (solid line). This function represents the WF of the resonance extremely well and is taken as the $^8$Be "bound state" wave function. Second, we argue that photodisintegration of $^9$Be proceeds entirely into the $^8$Be+$n$ channel. Indeed, one can estimate that, at small energies considered, the three–fragment $\alpha+\alpha+n$ disintegration channel is strongly suppressed due to the threshold regime. The experimental data also strongly supports the absence of this channel [12]. At the same time, the two–fragment $^4$He+$^5$He channel is still closed and ineffective due to the broad width of $^5$He. Thus our cross section starts from the $^8$Be+$n$ threshold of 1.6654 MeV. The cross section in the region between this threshold and the $\alpha\alpha n$ threshold of 1.5736 MeV is known to be tiny [19] and will be disregarded. As in the previous work (e.g. [20]) we confine ourselves to an s–wave relative $n^8$Be motion, i.e., with $1/2^+$ continuum states.

Predictions of the above dynamic $\alpha\alpha n$ model for the photodisintegration of $^9$Be depend crucially on the position of the excited state of $^9$Be with respect to the threshold. Preliminary three–body calculations gave us a peak lying too high in energy, and too broad. This could not be used for a reasonable fit to the data, so in the following we shall formulate an alternative representation of the continuum WF. We shall seek it in the form

$$\Psi_{\rm f} = \frac{1}{\sqrt{4\pi}} \frac{\phi^{^8{\rm Be}}(\rho)}{\rho} \frac{1}{\sqrt{4\pi}} \frac{\psi_{\rm sc}(r)}{r} \chi_{1/2}. \tag{2}$$

Here $\phi^{^8{\rm Be}}$ is the intrinsic wave function of $^8$Be calculated with the same $\alpha\alpha$ potential as for the ground state, and $\psi_{\rm sc}$ is the $n^8$Be relative motion function, where for large $r$ the normalization

$$\psi_{\rm sc}(r) \to \sin(kr + \delta) \tag{3}$$

is used.

Generally speaking, the true continuum wave function differs from (2) not only in the $n^8$Be interaction region but also in the outer region. However, at energies in the vicinity of the long–living excited state of $^9$Be the representation (2) should approximately be valid in the outer region. Indeed, the decay of the long–living state into the three–body $\alpha\alpha n$ channel is inhibited due to the threshold regime. Due to the approximate validity of the WF in (2) in the outer region one obtains a correct energy dependence of the cross section when using this WF. For small energies the main energy dependence of the transition matrix element appears as a factor in the continuum WF and is determined by an outer part of the WF, i.e. the phase shift. Besides, one can see below that just the outer region (where $\psi_{\rm sc}$ takes the form of (3)) gives the biggest contribution to the transition matrix element. One can therefore hope that a WF of the form of (2) suffices for the fitting purpose in the whole energy range considered.

We seek the relative motion function $\psi_{\rm sc}$ as a solution to the relative motion Schrödinger equation with some potential whose parameters are chosen from a fit of the theoretical cross section to the data. Taking into account that the s–wave $\alpha n$ repulsion and the p–wave $\alpha n$ attraction have comparable ranges one can assume a smooth attractive potential. The Woods–Saxon family

$$V(r) = -V_0 \left(1 + e^{\frac{r-R}{a}}\right)^{-1} \tag{4}$$

will be adopted below as a good representative.

Consider now the representation of the photodisintegration cross section in our model. The matrix element of the dipole transition operator $(4/9)e\mathbf{r}$ between the WFs in (1) and (2) has to be calculated. After integrating over $\rho$ the matrix element reduces to the overlap between the $n^8$Be relative motion functions, namely the scattering function entering (2) and the "effective bound state WF"

$$r^{-1}\psi_b(r)[Y_1(\hat{r})\chi_{1/2}]_{J=3/2} \tag{5}$$

obtained from (1):

$$r^{-1}\psi_b(r) = \int_0^\infty \phi_{011}(\rho, r)\rho d\rho \phi^{^8{\rm Be}}(\rho). \tag{6}$$

Using (2), (6) the cross section is of the same form as in the single–particle case. The total (s–wave) photodisintegration cross section is calculated in the simple form

$$\sigma = (2/3)^6 \pi (e^2/\hbar c)(2\mu/\hbar^2) E_\gamma k^{-1} I^2, \tag{7}$$

$$\text{where} \qquad I = \int_0^\infty \psi_{\rm b}(r)\psi_{\rm sc}(r) r dr. \tag{8}$$

Here $\mu$ is the $n^8$Be reduced mass, and $(\hbar k)^2/(2\mu)$ is the excitation energy $E_\gamma - E_{\rm th}$ that will be denoted as $E$ below. In case of a single–particle description of the process, i.e., the "valence neutron" model, (7) is valid with the bound–state WF normalized to unity, while in our case (see below)

$$\int_0^\infty \psi_{\rm b}^2(r)dr = 0.43. \qquad (9)$$

It is implied here and in (7) that the $^8$Be and $^9$Be ground state wave functions are normalized to unity. The function $\psi_{\rm b}(r)$ is shown in Fig. 2 (dashed line).

## III The photodisintegration cross section

In [21] the data at the energies up to 185 keV above threshold ($E_\gamma \leq 1.85$ MeV) from [13,14] were reproduced at a qualitative level within the following framework. The valence neutron model with Woods–Saxon type potentials was used. The results obtained in this way were multiplied by some constant factors less than unity, so called "reduction factors", to approach the experimental cross section. To obtain the continuum wave function the depth of the potential was varied while the radius and diffuseness parameters were taken the same as for the central component of the potential in the bound state calculation. Two fits were found, one with a reduction factor of 0.53 leading to a weakly bound $^8$Be+$n$ $1/2^+$ state, and the other one with a reduction factor of 0.31 leading to a virtual state. The first possibility was once preferred in view of the results of [22]. In that work a two channel $^8$Be+$n$ model of the ground state of $^9$Be was introduced to cure the single–particle description [20] of photodisintegration. The $^8$Be subsystem was allowed to be in the ground and first excited state, and that led to the reduction factor of 0.5 or 0.6 in the cross section depending on the assumptions. In [23] the reduction factor of 0.56 was found for that model. In contrast to [21] our results below definitely testify to a virtual $^8$Be+$n$ $1/2^+$ state. This is probably due to a more realistic treatment of the ground state of $^9$Be in our model. In fact the reduction factors obtained in the two–channel model of the ground state of $^9$Be [22] should be used in conjunction with the channel coupling n+$^8$Be dynamics, instead of using [21] single–channel dynamics.

In [24] the same data were fitted with the line shape $\sqrt{E}(E+\bar{E})^{-2}$. This shape was derived incorrectly from the Breit–Wigner cross section under the assumption that the $1/2^+$ level of $^9$Be is a bound or virtual $^8$Be+$n$ state. In [25] the data of [16] were fitted with a one–level R–matrix approximation. The fit leads to a complex–energy resonant state [25] and the real part of the complex energy proves to be negative.

First we shall analyze the data of [13–15] (full circles, full squares, and full diamond in Fig. 1). A search of the parameters $V_0$, $r$, and $a$ of the potential (4) giving an acceptable fit to the data is performed. Several local minima of the quantity $\chi^2$ in the space of the parameters

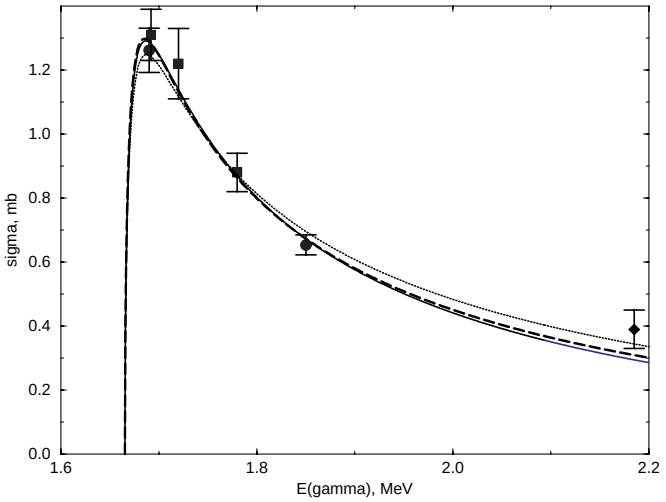


**Fig. 3.** Calculated cross sections for the photodisintegration of $^9$Be. *Solid* and *dashed curves* are obtained with the parameters (10) and (11), respectively. *Dotted curve* corresponds to the alternative method listed in the paragraph after Eq. (11). The experimental data are as in Fig. 1

are found. One of them is provided by

$$V_0 = 35.99\,{\rm MeV}, \quad R = 3.126\,{\rm fm}, \quad a = 0.8108\,{\rm fm}. \qquad (10)$$

These values seem to be very reasonable. For this set the $X = \chi^2/(\text{degrees of freedom})$ value equals 0.62. Another one is obtained with the parameters

$$V_0 = 52.86\,{\rm MeV}, \quad R = 2.006\,{\rm fm}, \quad a = 1.051\,{\rm fm} \qquad (11)$$

giving $X = 0.525$. Several other minima also exist with sizable higher but still acceptable $X$ values. In Fig. 3 the photodisintegration cross sections obtained with the parameters (10) and (11) are shown as the solid and dashed curve, respectively. The two cross sections prove to be quite close to each other. To clarify partially the reason for this we note that the biggest contribution to the matrix element of (8) comes from the distances beyond the range of the potential. The distances larger than 5 fm in (8) provide 60-70% contribution to the cross section, and at such distances the wave functions deviate from the asymptotic ones, (3), by not more than 10% (except for regions in the vicinity of zeros). The asymptotic wave functions are determined by the phase shifts i.e., predominantly by the scattering length $a$ and the effective range $r_0$. Therefore the procedure is equivalent to some degree to fitting $a$ and $r_0$ values. Once this is done, the cross sections are not very dependent on the particular set of the potential parameters. The $a$ and $r_0$ values are $-27.6$ fm and 8.79 fm, respectively, for the set (10), and $-28.4$ fm and 9.77 fm for the set (11). All the other above mentioned sets of potential parameters giving local minima to $X$ lead to very similar $a$ and $r_0$ values. However considerable changes in the scattering WF inside the potential can influence the results, see the next paragraph.

The following way to interpolate between the data has also been tried. Let us denote by $\sigma_0(E)$ the cross section

obtained in case when the right–hand side of (3) is used as a continuum wave function for all $r$ values. This cross section has been calculated taking $\delta$ from the effective range expansion with the $a$ and $r_0$ values given by the potential (10). Let us represent $\sigma$ as $c(E)\sigma_0(E)$ and fit $c(E)$ to experiment. It is hoped that, in contrast to $\sigma$, the factor $c(E)$ behaves in a smooth way and thus can be reliably obtained from an interpolation procedure. Indeed, the behavior of both $\sigma$ and $\sigma_0$ can be approximately described by the resonant factor $k^{-1}\sin^2\delta$ times a slowly varying function. Even a fit with $c(E) = const = 0.55$ proves to provide a sufficiently low $X$ value. The cross section obtained with this $c$ is shown in Fig. 3 as the dotted curve. Presumably this procedure provides less accurate results than the previous one. Of course, the energy dependence $k^{-1}\sin^2\delta$ is not accurate enough in the whole energy range, as a comparison with the exact solution for the potential (10) shows. Hence $c(E)$ should include an energy dependence, but this could not be determined because of experimental uncertainties.

Next we applied the procedure to the data of [16] (open circles in Fig. 1). Three local minima with acceptable $X$ values are found. However the parameters of the potential corresponding to all of them:

$$\begin{aligned} &V_0 = 11.0\,\mathrm{MeV}, \quad R = 2.35\,\mathrm{fm} \quad a = 0.258\,\mathrm{fm} \\ &V_0 = 6.49\,\mathrm{MeV}, \quad R = 3.10\,\mathrm{fm} \quad a = 0.260\,\mathrm{fm} \\ &V_0 = 15.8\,\mathrm{MeV}, \quad R = 1.37\,\mathrm{fm} \quad a = 0.958\,\mathrm{fm} \end{aligned} \tag{12}$$

prove to be rather unrealistic. There exists one more difference between these potentials and those in (10) and (11). The latter potentials, as well as the other potentials (4) providing a good fit to the same data, support one deeply bound state and one state close to being bound. On the contrary, the potentials (12) support only one very weakly bound state. An existence of one deeply bound $s$–level in the neutron mean field in the $^9$Be nucleus, or, equivalently, one node in the low–energy scattering wave function inside the potential, seems to be natural from the shell–model point of view. We think this point of view is sufficient to establish the correct number of nodes for the neutron motion inside the Woods–Saxon potential, even for such a clusterized system. In the $\alpha$–particle oscillator model of $^9$Be [26], for example, the first allowed neutron $s$–state contains a substantial admixture of the nodeless $0s$ function, but this leads not to a disappearance but only to a shift of the node. If one admits that the state considered is a mixture of $0s$ and $1s$ oscillator functions then there exists just one node located within the distance of 3 fm from the origin. Therefore we conclude that in the region where various data sets differ from each other the older radioactive isotope data are preferable. We also note that the cross section we obtain with potentials (10) and (11) for the highest energies considered, being lower than the fitted datum of Ref. [15], agrees well with the bremsstrahlung Jacobson data [11].

## IV The astrophysical reaction rates

The $^9\mathrm{Be}+\gamma \to \alpha+\alpha+n$ reaction rate per nucleus per time unit is calculated via the usual averaging the elementary photodisintegration cross section $\sigma(E_\gamma)c$ with the approximate, or Wien distribution for the photon density,

$$\lambda_\gamma = c\pi^{-2}(\hbar c)^{-3}\int_{E_{\mathrm{th}}(^8\mathrm{Be})}^{\infty}\sigma(E_\gamma)E_\gamma^2\exp(-E_\gamma/kT)dE_\gamma, \tag{13}$$

where $E_{\mathrm{th}}(^8\mathrm{Be}) = 1.6654$ MeV. The rate of the reverse reaction (the number of reactions per time unit per unit volume) is

$$P(\alpha\alpha n) = (1/2)n_\alpha^2 n_n\langle\alpha\alpha n\rangle, \tag{14}$$

where $n_\alpha$ and $n_n$ are numbers of particles per unit volume. The reaction constant $\langle\alpha\alpha n\rangle$ is obtained from (13) using the reverse ratio $RR$ [9,27]:

$$N_{\mathrm{A}}^2\langle\alpha\alpha n\rangle = \lambda_\gamma/RR, \tag{15}$$

$$RR = 5.84\cdot 10^{19}T_9^3\exp(-18.261/T^9). \tag{16}$$

Here $N_{\mathrm{A}}$ is Avogadro's number, $T_9$ is the temperature in $10^9$ K, $18.261/T^9 = E_{\mathrm{th}}(\alpha\alpha n)/kT$ with $E_{\mathrm{th}}(\alpha\alpha n) = 1.5736$ MeV, and it is implied that the quantities (13) and (15) are given in $\mathrm{sec}^{-1}$ and $\mathrm{cm}^6\ \mathrm{sec}^{-1}\ \mathrm{mole}^{-2}$, respectively. Use of the Wien distribution instead of the exact, or Planck, one, i.e. $[\exp(E_\gamma/kT)-1]^{-1} \to \exp(-E_\gamma/kT)$, allows application of the above listed simple reverse ratio theory. For temperatures of $T_9 = 5$ and 10, for example, it gives the reaction constant (13) with relative errors of 1 % and 5.4 %, respectively. For $E_\gamma \le 2.2$ MeV the cross section $\sigma(E_\gamma)$ obtained in the preceding section with the potential (10) is used. For $E_\gamma$ from 2.2 MeV up to 5 MeV the Jacobson bremsstrahlung data [11] are used. The former energy region provides 96% and 62% contribution to the cross section for $T_9 = 2$ and 5, respectively. The contribution from energies $E_\gamma$ higher than 5 MeV reaches 0.3% and 6.7% for $T_9 = 5$ and 8, respectively.

The values of the rate (15) obtained can be represented by the fit

$$N_A^2\langle\alpha\alpha n\rangle = 6.59\times 10^{-6}T_9^{-3/2} \exp[-(1.0653/T_9)]\left(1+\sum_{n=1}^{7}a_nT_9^n\right)^{-1} \tag{17}$$

with

$$\begin{aligned} &a_1 = 3.3562 \quad a_2 = -0.86389 \quad a_3 = 0.42268 \\ &a_4 = -0.14913 \quad a_5 = 2.7039\times 10^{-2} \\ &a_6 = -2.4000\times 10^{-3} \quad a_7 = 8.3223\times 10^{-5} \end{aligned}$$

The fit reproduces our $N_A^2\langle\alpha\alpha n\rangle$ values with an accuracy better than 1% at any $T_9$ in the range $0.1 \le T_9 \le 8$. In (17) $1.0653/T_9 = [E_{\mathrm{th}}(^8\mathrm{Be}) - E_{\mathrm{th}}(\alpha\alpha n)]/kT$. The factor $T_9^{-3/2}\exp[-(1.0653/T_9)]$ represents the asymptotic behavior of the $^8$Be formation contribution to the rate when $T_9$ tends to zero.

**Table 1.**

| $T$ [$10^9$ K] | $N_A^2\langle\alpha\alpha n\rangle$ | | | |
|---|---|---|---|---|
| | Present work | [9] | [6] (destructive) | [6] (constructive) |
| 0.2 | $0.21{\cdot}10^{-6}$ | $0.30{\cdot}10^{-6}$ | — | — |
| 0.5 | $0.87{\cdot}10^{-6}$ | $1.1{\cdot}10^{-6}$ | $0.55\cdot10^{-6}$ | $0.61\cdot10^{-6}$ |
| 1.0 | $0.60{\cdot}10^{-6}$ | $0.67{\cdot}10^{-6}$ | $0.32\cdot10^{-6}$ | $0.44\cdot10^{-6}$ |
| 2.0 | $0.23{\cdot}10^{-6}$ | $0.23{\cdot}10^{-6}$ | $0.12\cdot10^{-6}$ | $0.20\cdot10^{-6}$ |
| 3.0 | $0.12{\cdot}10^{-6}$ | $0.99{\cdot}10^{-7}$ | $0.60\cdot10^{-7}$ | $0.11\cdot10^{-6}$ |
| 4.0 | $0.73{\cdot}10^{-7}$ | $0.52{\cdot}10^{-7}$ | — | — |
| 5.0 | $0.51{\cdot}10^{-7}$ | $0.31{\cdot}10^{-7}$ | $0.26\cdot10^{-7}$ | $0.52\cdot10^{-7}$ |

In the Table our values for the three–body reaction rate (15) are compared with those of [9] and those of [6] where constructive or destructive interference between the resonant and non–resonant contributions at energies above the resonance energy was assumed.

Summarizing, we have constructed a semi–microscopic model for the low–energy photodisintegration of the $^9$Be nucleus and have analyzed the experimental data with its help. Our analysis supports the older radioactive isotope data. The theoretical cross section we derived may be compared with future microscopic calculations of the process. We have calculated the astrophysical rates for the reaction $\alpha+\alpha+n\rightarrow{}^9\mathrm{Be}+\gamma$ and the reverse reaction. Our new reaction rates agree at $T_9 = 2.0$ with the ones given in [9]. They are somewhat smaller (larger) for lower (higher) temperatures than $T_9 = 2.0$. The reaction rates given in [6] agree much better with our reaction rate at higher temperatures if one assumes in Ref. [6] constructive (destructive) interference between the resonant and non–resonant contributions at energies above (below) the resonance energy.

We are indebted to J.S. Vaagen and J.M. Bang for very fruitful comments. This work was supported partially by the the Fonds zur Förderung wissenschaftlichen Forschung in Österreich (project P10361–PHY) and the Russian Foundation for Basic Research (grant no 97-02-17003).

## V Appendix

In our calculation of the ground state of $^9$Be the $\alpha\alpha$ potential is taken in the form [28]

$$V_R\exp[-(\mu_R\rho)^2]-V_A\exp[-(\mu_A\rho)^2]$$

with $V_A = 130\,\mathrm{MeV}$, $\mu_A = 0.475\,\mathrm{fm}^{-1}$, $\mu_R = 0.7\,\mathrm{fm}^{-1}$, and $V_R = 500$, 320, and 10 MeV for $l$=0, 2, and 4, respectively. The Coulomb $\alpha\alpha$ interaction is also added. The $n\alpha$–interaction in s–, p–, and d–states is taken into account. As in many previous studies [30] the s–wave repulsive potential $V\exp[-(r/R)^2]$ with $V = 50\,\mathrm{MeV}$ and $R = 2.3\,\mathrm{fm}$ is used. The initial potential in p– and d–states [29] includes central and spin–orbit components:

$$V(r)=-V\left(1+e^{\frac{r-R}{a}}\right)^{-1}-U\,\mathbf{l}\cdot\mathbf{s}\,\frac{1}{r}\frac{d}{dr}\left(1+e^{\frac{r-R_1}{a_1}}\right)^{-1}$$

with $V = 43\,\mathrm{MeV}$, $R = 2\,\mathrm{fm}$, $a = 0.7\,\mathrm{fm}$, $U = 40\,\mathrm{MeV\,fm}^2$, $R_1 = 1.5\,\mathrm{fm}$, and $a_1$ =0.35 fm. The parameter $V$ is reduced to 39.6 MeV in the present three–body calculation, in order to reproduce the empirical g.s. energy.

The three–body dynamic equation is written in the form of the Faddeev differential equations and each Faddeev component is expanded over hyperspherical harmonics and hyperradial basis functions. Using the Raynal–Revai rotations of hyperspherical harmonics[3] the matrix elements are reduced analytically to two–dimensional integrals. The equations are projected onto subspaces of the basis functions retained that reduces the problem to the algebraic eigenvalue problem. The number of basis functions retained is quite high and ensures the adequate convergence of the calculation.

## References

1. A.S. Pudliner, V.R. Pandharipande, J. Carlson, S.C. Pieper, and R.B. Wiringa, Phys. Rev. C**56**, 1720 (1997)
2. K. Arai, Y. Ogawa, Y. Suzuki, and K. Varga, Phys. Rev. C**54**, 132 (1996)
3. S.E. Woosely, J.R. Wilson, G.J. Mathews, R.D. Hoffmann, and B.S. Meyer, Astrophys. J. **433**, 229 (1994)
4. K. Takahashi, J. Witti, and H.T. Janka, Astron. and Astrophys. **286**, 857 (1994)
5. S.E. Woosely and R.D. Hoffman, Astrophys. J. **395**, 202 (1992)
6. J. Görres, H. Herndl, I.J. Thompson, and M. Wiescher, Phys. Rev. C **52**, 2231 (1995)
7. V.D. Efros, W. Balogh, H. Herndl, R. Hofinger, and H. Oberhummer, Z. Phys. A **355**, 101 (1996)
8. H. Herndl, R. Hofinger, and H. Oberhummer, in Editors: S. Kubono and T. Kajino, Proceedings of the Symposium on Origin of Matter and Evolution of Galaxies 97 (OMEG97), Nov. 5-7, 1997, Atami, Japan, World Scientific, Singapore, in press
9. W.A. Fowler, G.R. Caughlan, and B.A. Zimmerman, Ann. Rev. Astron. Astrophys. **13**, 69 (1975)
10. F. Ajzenberg-Selove, Nucl. Phys. **A490**, 1 (1988)
11. M.J. Jacobson, Phys. Rev. **123**, 229 (1961)
12. B.L. Berman, R.L. Van Hemert, and C.D. Bowman, Phys. Rev. **163**, 958 (1967)

[3] A review of the hyperspherical formalism can be found e.g. in [30]

13. J.H. Gibbons, R.L. Maclin, J.B. Marion, and H.W. Schmitt, Phys. Rev. **114**, 1319 (1959)
14. W. John and J.M. Prosser, Phys. Rev. **127**, 231 (1962)
15. B. Hammermesh and C. Kimball, Phys. Rev. **90**, 1063 (1953)
16. M. Fuishiro, T. Tabata, K. Okamoto, and T. Tsuimoto, Can. J. Phys. **60**, 1672 (1982)
17. F.C. Barker and B.M. Fitzpatrick, Aust. J. Phys. **21** 415 (1968)
18. G.G. Ryzhih, R.A. Eramzhyan, V.I. Kukulin, and Yu.M. Tchuvilsky, Nucl. Phys. **A563**, 247 (1993)
19. M. Fuishiro, K. Okamoto, and T. Tsuimoto, Can. J. Phys. **61**, 1579 (1983)
20. N.C. Francis, D.T. Goldman, and E. Guth, Phys. Rev. **120**, 2175 (1960)
21. E.G. Corman, J.E. Sherwood, and W. John, Phys. Lett. **4**, 146 (1963)
22. J.S. Blair, Phys. Rev. **123**, 2151 (1961)
23. F.C. Barker, Nucl. Phys. **28**, 96 (1961)
24. C. Mahaux, Nucl. Phys. **71**, 241 (1965)
25. F.C. Barker, Can. J. Phys. **61**, 1371 (1983)
26. P.D. Kunz, Ann. Phys. **11**, 275 (1960)
27. W.A. Fowler, G.R. Caughlan, and B.A. Zimmerman, Ann. Rev. Astron. Astrophys. **13**, 69 (1975)
28. S. Ali and A.R. Bodmer, Nucl. Phys. **80**, 99 (1966)
29. J. Bang and C. Gignoux, Nucl. Phys. **A313**, 119 (1979)
30. M.V. Zhukov, B.V. Danilin, D.V. Fedorov, J.M. Bang, I.J. Thompson, and J.S. Vaagen, Phys. Rep. **231**, 151 (1993)